

Supporting Information

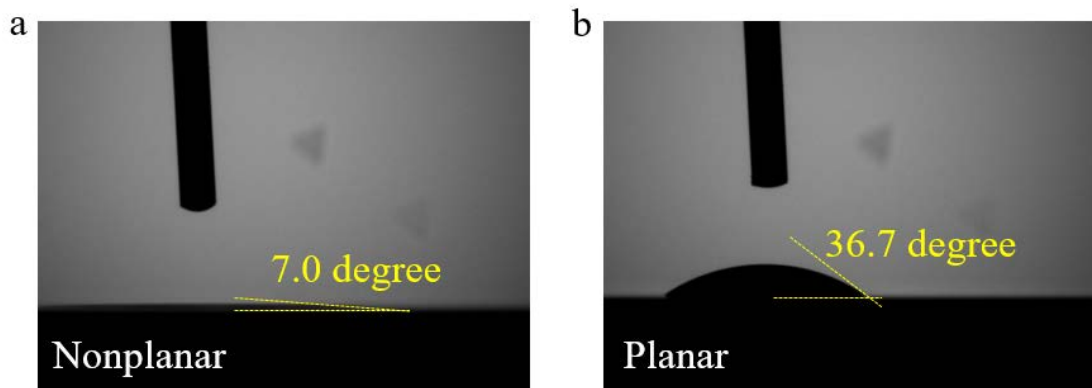
**A quadruple-band metal-nitride nanowire artificial
photosynthesis system for high efficiency photocatalytic overall
solar water splitting**

Yongjie Wang¹, Yuanpeng Wu¹, Kai Sun², and Zetian Mi^{1,*}

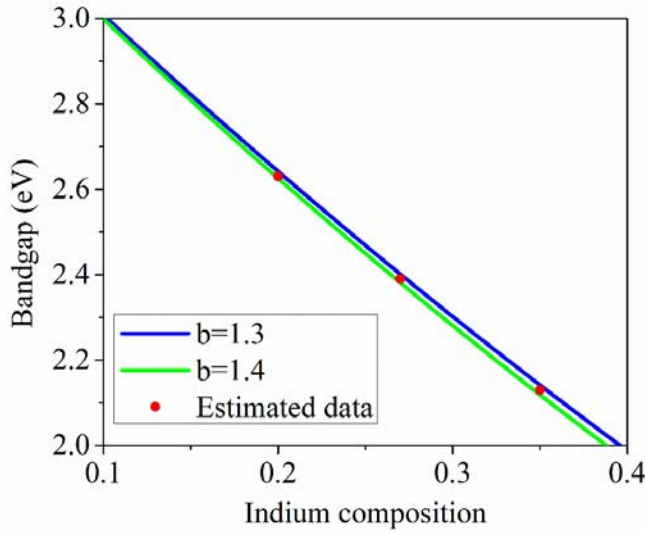
*¹Department of Electrical Engineering and Computer Science, University of Michigan,
1301 Beal Avenue, Ann Arbor, Michigan 48109, USA*

*²Department of Materials Science and Engineering, University of Michigan, 2300
Hayward Street, Ann Arbor, Michigan 48109, USA*

**Corresponding author: ztmi@umich.edu*



Supplementary Figure S1. Contact angle measurements using pure water droplets on metal nitride nanowires grown on a nonplanar Si wafer (a) and a planar Si wafer (b). The water contact angle can be greatly reduced by using nonplanar substrates indicating the improved hydrophilic property.



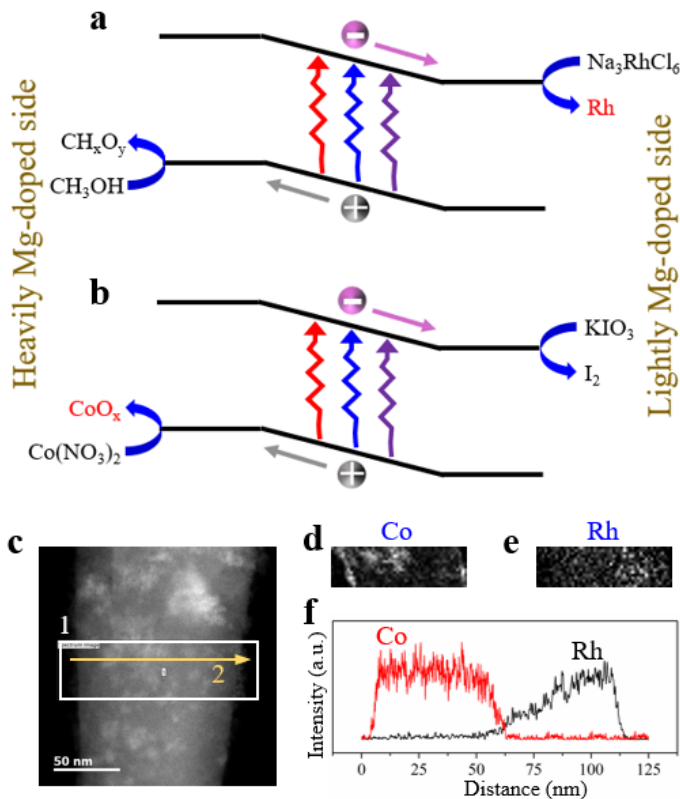
Supplementary Figure S2. Estimated indium compositions of InGaN nanowires using the Vegard's law with a bowing parameter b of 1.3 and 1.4.

For $\text{In}_x\text{Ga}_{1-x}\text{N}$ alloy with varied indium incorporations, the Vegard's law correlates its bandgap and indium composition with the Eqn. S1 below.

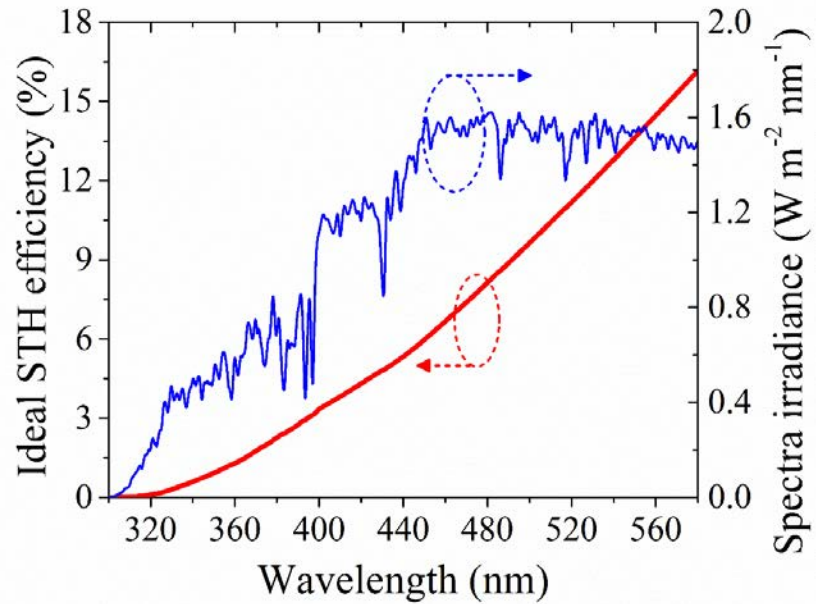
$$E_g(\text{In}_x\text{Ga}_{1-x}\text{N}) = x \cdot E_g(\text{InN}) + (1 - x) \cdot E_g(\text{GaN}) - b \cdot x \cdot (1 - x) \quad (\text{S1})$$

where b is the bowing parameter and its value typically varies between 1.3 and 1.4.¹⁻⁴

In this study, the bandgaps of InGaN nanowires have been determined from photoluminescence measurements to be ~2.6 eV, ~2.4 eV, and ~2.1 eV, respectively, as shown in Figure 2c. Therefore, its indium compositions were estimated to be ~0.2, ~0.27, and ~0.35, respectively, using Eqn. S1.



Supplementary Figure S3. Schematic illustration of cocatalyst nanoparticles deposition on InGaN nanowires, wherein (a) Rh deposits on lightly doped surface from reduction reaction, and (b) Co_xO deposits on heavily doped surface from oxidation reaction. (c) Dark-field scanning transmission electron microscope (DF-STEM) image of InGaN nanowire after cocatalyst deposition. Elemental distribution of Co (d) and Rh (e) using energy-dispersive X-ray spectroscopy (EDX) in the marked area in (c). (f) Line scanning showing the separate deposition of Co and Rh along Arrow 2 marked in (c).



Supplementary Figure S4. The theoretical maximum solar-to-hydrogen (STH) conversion efficiency for the ideal multi-band photocatalyst system absorbing photons with wavelengths up to 580 nm, wherein all the incident photons are assumed to drive water splitting reaction.⁵

Supplementary Note S1. Solar-to-hydrogen conversion efficiency calculation

For overall water splitting, the solar-to-hydrogen (STH) conversion efficiency is defined as the chemical energy of generated H₂ gas divided by the solar energy of incident light. The STH efficiency for photocatalytic water splitting devices can be calculated by Eqn. S2 using the Gibbs free energy (237 kJ mol⁻¹) of H₂.⁶ To obtain STH efficiency correctly, it is required to demonstrate the stoichiometric H₂ and O₂ gas evolution, without adding any sacrificial reagents.

$$\text{STH} = \left[\frac{\text{H}_2 \text{ generation rate (mmol s}^{-1}\text{)} \times 237000 \text{ J mol}^{-1}}{\text{Incident solar power (mW cm}^{-2}\text{)} \times \text{Area (cm}^2\text{)}} \right]_{\text{AM1.5G}} \quad (\text{S2})$$

The incident solar power from Xenon lamp with AM 1.5G filter was measured to be 2329 mW cm⁻² by a thermopile detector (919P, Newport).

Quadruple-band InGaN nanowires for pure water splitting

$$\text{STH} = \left[\frac{(1.84/3600 \text{ mmol s}^{-1}) \times 237000 \text{ J mol}^{-1}}{(2329 \text{ mW cm}^{-2}) \times (1 \text{ cm}^2)} \right]_{\text{AM1.5G}} = \sim 5.2\%$$

Supplementary Table S1. STH efficiency and stability of some previously reported photocatalyst systems for overall solar water splitting, compared to the multi-band InGaN nanowires presented in this work.

Materials	Cocatalyst	Electrolyte	Light	STH (%)	Stability (hours)	Year [Ref.]
Multi-band InGaN nanowires	Rh/CrO _x - CoO _x	Pure water	23 suns	5.2	8	This work
Double-band In _{0.22} Ga _{0.78} N/GaN	Rh/CrO _x	Pure water	32 suns	3.3	2	2018 [7]
SrTiO ₃ :Al	Rh/CrO _x	Pure water	300W Xe lamp	0.4	4	2018 [8]
CDs/CdS-S	N/A	Seawater	One sun	<0.1	90	2018 [9]
Double-band In _{0.25} Ga _{0.75} N/GaN	Rh/CrO _x - CoO _x	Seawater	27 suns	1.9	3	2018 [10]
MoS ₂ /TiO ₂	N/A	Pure water methanol	One sun	<1	21	2018 [11]
TiO ₂ :Ta/N SrTiO ₃ :Rh	Ru - RuO _x	1 mM NaIO ₃ 1 mM FeCl ₃	One sun	0.02	15	2017 [12]
SrTiO ₃ :La, Rh/C /BiVO ₄ :Mo	Ru - RuO _x	Pure water	One sun	1.2	6	2017 [13]
Bi ₄ NbO ₈ Cl SrTiO ₃ :Rh	Pt - RuO _x	Fe ³⁺ /Fe ²⁺ redox	300W Xe lamp	<0.4	24	2016 [14]
SrTiO ₃ :La, Rh/Au /BiVO ₄ :Mo	Ru/Cr ₂ O ₃ /a-TiO ₂	Pure water	One sun	1.1	10	2016 [15]
GaN nanowires	Rh/CrO _x	Pure water	27 suns	<1	22	2015 [16]
CDots/C ₃ N ₄	N/A	Pure water	1 sun	2	200 days	2015 [17]
SrTiO ₃ : Rh, Sb BiVO ₄ :Mo	IrO ₂ /CoO _x	1 mM H ₂ SO ₄	300W Xe lamp	0.01	30	2014 [18]
CoO nanoparticles Si/TiO ₂	N/A Pt - IrO _x	Pure water 0.5 M H ₂ SO ₄	One sun 1.5 suns	5 0.12	0.5 4.5	2013 [19] 2013 [20]

Supplementary references

- 1 Y. Wang; S. Vanka; J. Gim; Y. Wu; R. Fan; Y. Zhang; J. Shi; M. Shen; R. Hovden; Z. Mi, *Nano Energy*, 2019, **57**, 405-413.
- 2 R. R. Pelá; C. Caetano; M. Marques; L. G. Ferreira; J. Furthmüller; L. K. Teles, *Appl. Phys. Lett.*, 2011, **98**, 151907.
- 3 T. Kuykendall; P. Ulrich; S. Aloni; P. Yang, *Nat. Mater.*, 2007, **6**, 951.
- 4 I. Vurgaftman; J. R. Meyer, *J. Appl. Phys.*, 2003, **94**, 3675-3696.
- 5 Y. Wang; S. Zhao; Y. Wang; D. A. Laleyan; Y. Wu; B. Ouyang; P. Ou; J. Song; Z. Mi, *Nano Energy*, 2018, **51**, 54-60.
- 6 Z. Chen; H. Dinh; E. Miller, *Photoelectrochemical water splitting: Standards, experimental methods, and protocols*. Springer-Verlag New York: 2013.
- 7 F. A. Chowdhury; M. L. Trudeau; H. Guo; Z. Mi, *Nat. Commun.*, 2018, **9**, 1707.
- 8 Y. Goto; T. Hisatomi; Q. Wang; T. Higashi; K. Ishikiriyama; T. Maeda; Y. Sakata; S. Okunaka; H. Tokudome; M. Katayama; S. Akiyama; H. Nishiyama; Y. Inoue; T. Takewaki; T. Setoyama; T. Minegishi; T. Takata; T. Yamada; K. Domen, *Joule*, 2018, **2**, 509-520.
- 9 C. Zhu; C. a. Liu; Y. Fu; J. Gao; H. Huang; Y. Liu; Z. Kang, *Appl. Catal. B*, 2019, **242**, 178-185.
- 10 X. Guan; F. A. Chowdhury; N. Pant; L. Guo; L. Vayssieres; Z. Mi, *J. Phys. Chem. C*, 2018, **122**, 13797-13802.
- 11 L. Guo; Z. Yang; K. Marcus; Z. Li; B. Luo; L. Zhou; X. Wang; Y. Du; Y. Yang, *Energy Environ. Sci.*, 2018, **11**, 106-114.

- 12 A. Nakada; S. Nishioka; J. J. M. Vequizo; K. Muraoka; T. Kanazawa; A. Yamakata;
S. Nozawa; H. Kumagai; S.-i. Adachi; O. Ishitani; K. Maeda, *J. Mater. Chem. A*,
2017, **5**, 11710-11719.
- 13 Q. Wang; T. Hisatomi; Y. Suzuki; Z. Pan; J. Seo; M. Katayama; T. Minegishi; H.
Nishiyama; T. Takata; K. Seki; A. Kudo; T. Yamada; K. Domen, *J. Am. Chem.
Soc.*, 2017, **139**, 1675-1683.
- 14 H. Fujito; H. Kunioku; D. Kato; H. Suzuki; M. Higashi; H. Kageyama; R. Abe, *J.
Am. Chem. Soc.*, 2016, **138**, 2082-2085.
- 15 Q. Wang; T. Hisatomi; Q. Jia; H. Tokudome; M. Zhong; C. Wang; Z. Pan; T.
Takata; M. Nakabayashi; N. Shibata; Y. Li; I. D. Sharp; A. Kudo; T. Yamada; K.
Domen, *Nat. Mater.*, 2016, **15**, 611.
- 16 M. G. Kibria; S. Zhao; F. A. Chowdhury; Q. Wang; H. P. T. Nguyen; M. L. Trudeau;
H. Guo; Z. Mi, *Nat. Commun.*, 2014, **5**, 3825.
- 17 J. Liu; Y. Liu; N. Liu; Y. Han; X. Zhang; H. Huang; Y. Lifshitz; S.-T. Lee; J. Zhong;
Z. Kang, *Science*, 2015, **347**, 970.
- 18 R. Asai; H. Nemoto; Q. Jia; K. Saito; A. Iwase; A. Kudo, *Chem. Commun.*, 2014,
50, 2543-2546.
- 19 L. Liao; Q. Zhang; Z. Su; Z. Zhao; Y. Wang; Y. Li; X. Lu; D. Wei; G. Feng; Q. Yu;
X. Cai; J. Zhao; Z. Ren; H. Fang; F. Robles-Hernandez; S. Baldelli; J. Bao, *Nat.
Nanotechnol.*, 2013, **9**, 69.
- 20 C. Liu; J. Tang; H. M. Chen; B. Liu; P. Yang, *Nano Lett.*, 2013, **13**, 2989-2992.